

Linear viscoelasticity of polyolefin melts: the effects of temperature and chain branching

A.D. Drozdov*, S. Agarwal and R.K. Gupta
Department of Chemical Engineering
West Virginia University
P.O. Box 6102
Morgantown, WV 26506, USA

Abstract

Observations are reported in isothermal torsional oscillation tests on melts of isotactic polypropylene (iPP) and low-density polyethylene (LDPE) in the intervals of temperature between 190 and 250 °C (iPP) and between 120 and 190 °C (LDPE). With reference to the concept of transient networks, constitutive equations are developed for the viscoelastic response of polymer melts at three-dimensional deformations with small strains. A melt is treated as an equivalent network of strands bridged by temporary junctions (entanglements and physical cross-links whose life-times exceed the characteristic time of deformation). The time-dependent behavior of the network is modelled as detachment of active strands from their junctions and merging of dangling strands with the network. The network is assumed to be strongly heterogeneous in the sense that different junctions have different activation energies for separation of strands. The stress-strain relations involve three adjustable parameters (the plateau modulus, the average activation energy for rearrangement of strands and the standard deviation of activation energies) that are determined by matching the dependencies of storage and loss moduli on frequency of oscillations. The difference in the effects of temperature on the material constants of iPP and LDPE is associated with the difference in their molecular architecture.

Key-words: Isotactic polypropylene, Low-density polyethylene, Viscoelasticity, Thermal properties, Chain branching

*Corresponding author; Fax: (304) 293 4139; E-mail: Aleksey.Drozdov@mail.wvu.edu

1 Introduction

This paper is concerned with the effect of temperature on the viscoelastic response of melts of isotactic polypropylene (iPP) and low-density polyethylene (LDPE). The choice of these polyolefins for the investigation may be explained by two reasons. First, polyethylene and polypropylene are conventional polymers widely used in industrial applications: oriented films for packaging, reinforcing fibres, non-woven fabrics, pipes, etc., as well as components of copolymers and blends with improved mechanical properties. Secondly, these polymers have a similar structure of backbones (polypropylene differs from polyethylene by the presence of methyl side-groups only), but quite different molecular architecture (relatively short-branched chains in iPP versus long-branched chains in LDPE). The aim of the present work is to shed some light on relations between the micro-structure of an ensemble of macromolecules on the one hand, and the time-dependent behavior of polymer melts observed in conventional torsional oscillatory tests, on the other. In particular, we focus on the effects of long chain branches on the evolution of (i) the shear modulus of a melt and (ii) its characteristic relaxation time with temperature.

According to the theory of entropic elasticity (Ferry, 1980), the elastic modulus μ of a flexible chain linearly increases with the absolute temperature T ,

$$\mu = \mu_0 k_B T, \quad (1)$$

where k_B is Boltzmann's constant, and the dimensionless coefficient μ_0 is of order of unity (this coefficient is determined by an averaging method in the calculation of the chain's entropy). As conventional concepts in rubber elasticity disregard interactions between chains (these interactions are accounted for by means of the incompressibility condition), the shear modulus of an ensemble of polymer chains equals the product of the concentration of strands (segments of macromolecules between contiguous junctions) per unit mass N by the elastic modulus of an individual chain μ ,

$$G = \rho \mu N, \quad (2)$$

where ρ stands for mass density. For linear chains, the number of strands per unit mass N equals the product of the number of chains per unit mass \mathcal{N} by the average number of strands per chain β ,

$$N = \beta \mathcal{N}, \quad \beta = \frac{L}{L_e}. \quad (3)$$

Here L is the average contour length of a chain, and L_e is the average contour length between entanglements. Combining Eqs. (1) to (3), we arrive at the conventional formula

$$G = \rho \mu_0 k_B \mathcal{N} L \frac{T}{L_e}. \quad (4)$$

Experimental data demonstrate a pronounced decrease of the apparent elastic modulus (defined, e.g., as the storage modulus G' measured at the maximal frequency ω_{\max} available in an experiment) with temperature T (see Figures 1 and 3 below). As all parameters on the right-hand side of Eq. (4) but the ratio T/L_e are temperature independent (insignificant changes in density with temperature are disregarded in the present study), this implies that the average contour length between entanglements L_e strongly increases with temperature,

$$L_e(T) = C l_e(T), \quad l_e(T) = \frac{T}{G(T)}, \quad C = \rho \mu_0 k_B \mathcal{N} L. \quad (5)$$

For an ensemble of linear chains, the growth of L_e with temperature T may be attributed to an increase in the average inter-chain distance driven by activation of thermal fluctuations. The same process determines an increase in the specific volume (length) with temperature, which is described by the conventional equation

$$\frac{1}{l} \frac{dl}{dT} = \alpha, \quad (6)$$

where l denotes a characteristic length, and α is the coefficient of linear thermal expansion. Based on this similarity, we propose to describe changes in $l_e(T)$ by the differential equation similar to Eq. (6),

$$\frac{1}{l_e - l_e^{(0)}} \frac{dl_e}{dT} = \alpha_e, \quad (7)$$

where α_e stands for an analog of the coefficient of linear thermal expansion for the average length between entanglements, and $l_e^{(0)}$ characterizes the contour length between entanglements at relatively low temperatures T . Solving Eq. (7) for a constant coefficient α_e , we find that

$$l_e(T) = l_e^{(0)} + l_e^{(1)} \exp\left(\frac{T}{T_e}\right), \quad T_e = \frac{1}{\alpha_e}. \quad (8)$$

Combining Eqs. (5) and (8), we arrive at the formula for the shear modulus G as a function of temperature T ,

$$G(T) = \frac{T}{l_e^{(0)} + l_e^{(1)} \exp(T/T_e)}. \quad (9)$$

It is worth noting that an equation similar to Eq. (9) (where the coefficient $l_e^{(0)}$ is absent) has recently been proposed by Wood-Adams and Costeux (2001) based on another physical ground.

A substantial increase in the entanglement distance l_e with temperature T has been observed by Richter et al. (1990, 1993) about a decade ago by using neutron spin-echo spectroscopy (NSES) in polyisoprene, polybutadiene and a poly(ethylene–propylene) alternative copolymer. To the best of our knowledge, no attempts have been made, however, to model the growth of $l_e(T)$ with the help of differential equations, as well as to evaluate their parameters by matching observations in rheological tests. The latter may be explained by the use of conventional methods (Ferry, 1980) for determining the plateau modulus G° (an analog of the instantaneous modulus G). These methods are grounded on shifting the graphs of the storage modulus G' measured at various temperatures T and plotted in the double-logarithmic coordinates as functions of frequency ω along both axes: no restrictions are imposed on the shift along the abscissa axis (which characterizes the shift factor), whereas an appropriate shift along the ordinate axis is presumed to be proportional to the logarithm of temperature T , which is tantamount to formula (2) with a constant N .

The objective of this study is two-fold:

- to develop a constitutive model for the isothermal time-dependent response of a polymer melt at small strains that involves only three material constants (including the instantaneous shear modulus G),
- to report experimental data in torsional oscillation tests on isotactic polypropylene and low-density polyethylene at various temperatures T , to determine adjustable parameters in the stress–strain relations by fitting the observations, and to verify Eq. (9) by comparing the experimental data with the results of numerical simulation.

To develop constitutive equations tractable from the mathematical standpoint, we adopt a homogenization concept. According to it, a complicated micro-structure of a polymer melt is replaced by an equivalent phase, whose response captures essential features of the mechanical behavior. Following common practice (Sweeney et al., 1999), a network of chains is chosen as an equivalent phase.

The time-dependent behavior of melts is modelled within the concept of transient networks (Green and Tobolsky, 1946; Yamamoto, 1956; Lodge, 1968; Tanaka and Edwards, 1992). A polymer melt is thought of as a network of strands bridged by temporary junctions (entanglements and physical cross-links whose life-time exceeds the characteristic time of rheological tests). It is assumed that active strands (whose ends are linked to contiguous junctions) separate from these junctions, while dangling strands (that have a free end) merge with the network. Detachment and attachment events occur at random times as appropriate strands are excited by thermal fluctuations. Following Drozdov and Christiansen (2003), we assume the network to be strongly heterogeneous in the sense that different junctions have different activation energies for detachment of active strands. The inhomogeneity of the network is attributed to (i) density fluctuations in the ensemble of macromolecules, and (ii) the fact that the life-time of entanglements created by long branches as well as formed by backbones but located in the neighborhoods of chain's ends is smaller than that of knots between backbones of different macromolecules entangled in the vicinity of their middle-points. The distribution of active strands with various activation energies for rearrangement is described by the random energy model (Derrida, 1980).

The stress-strain relations involve three adjustable parameters: (i) the instantaneous modulus G , (ii) the average activation energy for separation of strands from temporary junctions V_* , and (iii) the standard deviation of activation energies Σ_* , which, in general, depend on temperature T . These quantities are found by fitting experimental data for the storage and loss moduli in shear oscillatory tests at each temperature separately. This procedure provides an opportunity to evaluate the dependence $G(T)$ and to verify Eq. (9).

The exposition is organized as follows. Experimental data in torsional oscillation tests are reported in Section 2. Constitutive equations for an heterogeneous transient network of strands at three-dimensional deformations are derived in Section 3. Adjustable parameters in the stress-strain relations are determined in Section 4. A brief discussion of our findings is given in Section 5. Some concluding remarks are formulated in Section 6.

2 Experimental procedure

Isotactic polypropylene PP 1012 (density 0.906 g/cm³, melt flow rate 1.2 g/10 min) was purchased from BP Amoco Polymers, Inc. Low-density polyethylene Huntsman PE 1020 (density 0.923 g/cm³, melt flow rate 2.0 g/10 min) was supplied by GE Company. Granules were dried at the temperature $T = 100$ °C for 12 h prior to molding. Circular plates with radius 62 mm and thickness 3 mm were molded in injection-molding machine Battenfeld 1000/315 CDC (Battenfeld). Specimens for rheological tests (with diameter 30 mm) were cut from the plates.

To evaluate melting temperatures of iPP and LDPE, DSC (differential scanning calorimetry) measurements were carried out by using DSC 910S apparatus (TA Instruments). The calorimeter was calibrated with indium as a standard. Two specimens of each polymer with

weights of approximately 15 mg were tested with a heating rate of 10 K/min from room temperature to 200 °C. The melting temperatures $T_m = 172$ (iPP) and $T_m = 113$ °C (LDPE) were determined as the point corresponding to the peaks on the melting curves.

Rheological tests were performed by using RMS-800 rheometric mechanical spectrometer with parallel disks (diameter 25 mm, gap length 2 mm) at the temperatures $T = 190, 210, 230$ and 250 °C (iPP) and $T = 120, 130, 140, 150, 160, 170, 180$ and 190 °C (LDPE). Given a temperature T , at least two dynamic tests were carried out on different samples. The shear storage modulus G' and the shear loss modulus G'' were measured in oscillation tests (the frequency-sweep mode) with the amplitude of 15 % and various frequencies ω ranging from 0.1 to 100 rad/s. Our choice of the amplitude of oscillations was based by the following requirements: (i) mechanical tests were performed in the region of linear viscoelasticity, and (ii) the torque was less than its ultimate value 0.2 N·m. The limitation on the minimum frequency of oscillations was imposed by two conditions: (i) the torque exceeded its minimum value $2.0 \cdot 10^{-4}$ N·m, and (ii) the duration of a test did not exceed 20 min, which ensured that thermal degradation of polymers at elevated temperatures may be disregarded. To check that the storage and loss moduli were not affected by the strain amplitude, several tests were repeated with the amplitude of 5 %; no changes in dynamic moduli were observed. The temperature in the chamber was controlled with a standard thermocouple that indicated that the temperature of specimens remained practically constant (with the accuracy of ± 1.0 °C).

Each test was performed on a new sample. The specimen was thermally equilibrated in the spectrometer (during 5 min), the gap length was reduced to 2 mm, an extraneous material was carefully removed, and the storage and loss moduli were measured at various frequencies ω starting from the lowest one.

The storage G' and loss G'' moduli are depicted versus the logarithm ($\log = \log_{10}$) of frequency ω in Figures 1 and 2 for iPP and in Figures 3 and 4 for LDPE. Conventional semi-logarithmic plots are used to characterize changes in these quantities with frequency. According to Figures 1 to 4, the dependencies of storage and loss moduli on frequency of oscillations have similar shapes for both polyolefins. Given a temperature T , the storage modulus G' and the loss modulus G'' strongly increase with frequency ω . For a fixed frequency ω , the dynamic moduli pronouncedly decrease with temperature T .

3 Constitutive equations

With reference to the concept of transient networks, a polymer melt is thought of as an equivalent network of strands bridged by temporary junctions. A strand whose ends are linked to contiguous junctions is treated as an active one. When an end of an active strand separates from a junction, the strand is transformed into the dangling state. When a free end of a dangling strand captures a nearby junction, the strand returns into the active state. Separation of active strands from their junctions and merging of dangling strands with the network occur at random times when the strands are excited by thermal fluctuations. According to the theory of thermally-activated processes (Eyring, 1936), the rate of detachment of strands from temporary junctions Γ is governed by the equation

$$\Gamma = \Gamma_0 \exp\left(-\frac{\bar{v}}{k_B T}\right), \quad (10)$$

where Γ_0 is the attempt rate (the number of separation events per strand per unit time), k_B is Boltzmann's constant, T is the absolute temperature, and $\bar{v} \geq 0$ is the activation energy for separation of an active strand. In what follows, we set $\Gamma_0 = 10^{11} \text{ s}^{-1}$, which corresponds to the characteristic relaxation rate at the monomeric scale (deGennes, 1979).

For isothermal deformation at a temperature T , we introduce the dimensionless activation energy

$$v = \frac{\bar{v}}{k_B T}, \quad (11)$$

and present Eq. (10) in the form

$$\Gamma(v) = \Gamma_0 \exp(-v). \quad (12)$$

To describe the time-dependent response of a melt, we suppose that different junctions are characterized by different dimensionless activation energies v (Drozdov and Christiansen, 2003). The distribution of active strands in a transient network is determined by the number of active strands per unit mass N and the distribution function $p(v)$. The quantity $Np(v)dv$ equals the number of active strands per unit mass linked to junctions with the dimensionless activation energies u belonging to the interval $[v, v + dv]$.

Separation of active strands from temporary junctions and merging of dangling strands with the network are entirely described by the function $n(t, \tau, v)$ that equals the number (per unit mass) of active strands at time $t \geq 0$ linked to temporary junctions with activation energy v which have last merged with the network before instant $\tau \in [0, t]$.

The quantity $n(t, t, v)$ equals the number of active strands (per unit mass) with the activation energy v at time t ,

$$n(t, t, v) = Np(v). \quad (13)$$

The function

$$\gamma(\tau, v) = \left. \frac{\partial n}{\partial \tau}(t, \tau, v) \right|_{t=\tau} \quad (14)$$

determines the rate of reformation for dangling chains: the amount $\gamma(\tau, v)d\tau$ equals the number of dangling strands (per unit mass) that merge with temporary junctions with activation energy v within the interval $[\tau, \tau + d\tau]$. The quantity

$$\frac{\partial n}{\partial \tau}(t, \tau, v) d\tau$$

is the number of these strands that have not separated from their junctions during the interval $[\tau, t]$. The amount

$$-\frac{\partial n}{\partial t}(t, 0, v) dt$$

is the number of active strands (per unit mass) that detach (for the first time) from the network within the interval $[t, t + dt]$, while the quantity

$$-\frac{\partial^2 n}{\partial t \partial \tau}(t, \tau, v) dt d\tau$$

equals the number of strands (per unit mass) that have last merged with the network within the interval $[\tau, \tau + d\tau]$ and separate from the network (for the first time after merging) during the interval $[t, t + dt]$.

The rate of detachment Γ is defined as the ratio of the number of active strands that separate from temporary junctions per unit time to the total number of active strands. Applying this definition to active strands that were connected with the network at the initial instant $t = 0$, and to those that merged with the network within the interval $[\tau, \tau + d\tau]$, we arrive at the differential equations

$$\frac{\partial n}{\partial t}(t, 0, v) = -\Gamma(v)n(t, 0, v), \quad \frac{\partial^2 n}{\partial t \partial \tau}(t, \tau, v) = -\Gamma(v)\frac{\partial n}{\partial \tau}(t, \tau, v). \quad (15)$$

Integration of Eq. (15) with initial conditions (13) (where we set $t = 0$) and (14) implies that

$$n(t, 0, v) = Np(v) \exp[-\Gamma(v)t], \quad \frac{\partial n}{\partial \tau}(t, \tau, v) = \gamma(\tau, v) \exp[-\Gamma(v)(t - \tau)]. \quad (16)$$

To exclude the function $\gamma(t, v)$ from Eq. (16), we use the identity

$$n(t, t, v) = n(t, 0, v) + \int_0^t \frac{\partial n}{\partial \tau}(t, \tau, v) d\tau. \quad (17)$$

Substitution of expressions (13) and (16) into Eq. (17) results in

$$Np(v) = Np(v) \exp[-\Gamma(v)t] + \int_0^t \gamma(\tau, v) \exp[-\Gamma(v)(t - \tau)] d\tau. \quad (18)$$

The solution of linear integral equation (18) reads $\gamma(t, v) = Np(v)\Gamma(v)$. It follows from this equality and Eq. (16) that

$$\frac{\partial n}{\partial \tau}(t, \tau, v) = Np(v)\Gamma(v) \exp[-\Gamma(v)(t - \tau)]. \quad (19)$$

We adopt the conventional assumptions that (i) the excluded-volume effect and other multi-chain effects are screened for individual strands by surrounding macromolecules, (ii) the energy of interaction between strands can be taken into account with the help of the incompressibility condition, and (iii) thermal oscillations of junctions can be disregarded, and the strain tensor for the motion of junctions at the micro-level coincides with the strain tensor for macro-deformation.

At isothermal deformation with small strains, a strand is treated as an isotropic incompressible medium with the strain energy

$$w_0 = \mu \hat{e}' : \hat{e}',$$

where \hat{e} is the strain tensor for transition from the reference (stress-free) state of the strand to its deformed state, the average elastic modulus μ is given by Eq. (1), the prime stands for the deviatoric component of a tensor, and the colon denotes convolution of two tensors.

According to the affinity hypothesis, the strain energy $\bar{w}_0(t, 0)$ of an active strand that has not separated from the network during the interval $[0, t]$ reads

$$w(t, 0) = \mu \hat{e}'(t) : \hat{e}'(t),$$

where $\hat{e}(t)$ is the strain tensor for transition from the initial (stress-free) state of the network to its deformed state at time t . With reference to Tanaka and Edwards (1992), we suppose

that stress in a dangling strand totally relaxes before this strand captures a new junction. This implies that the stress-free state of an active strand that merges with the network at time $\tau \geq 0$ coincides with the deformed state of the network at that instant. The strain energy of an active strand that has last merged with the network at time $\tau \in [0, t]$ is given by

$$w(t, \tau) = \mu [\hat{\epsilon}(t) - \hat{\epsilon}(\tau)]' : [\hat{\epsilon}(t) - \hat{\epsilon}(\tau)]'.$$

Multiplying the strain energy per strand by the number of active strands per unit mass and summing the mechanical energies of active strands linked to temporary junctions with various activation energies, we find the strain energy per unit mass of an equivalent network

$$W(t) = \mu \int_0^\infty \left\{ n(t, 0, v) \dot{\epsilon}'(t) : \dot{\epsilon}'(t) + \int_0^t \frac{\partial n}{\partial \tau}(t, \tau, v) [\hat{\epsilon}(t) - \hat{\epsilon}(\tau)]' : [\hat{\epsilon}(t) - \hat{\epsilon}(\tau)]' d\tau \right\} dv. \quad (20)$$

Differentiating Eq. (20) with respect to time t and using Eqs. (16) and (19), we arrive at the formula

$$\frac{dW}{dt}(t) = \hat{A}'(t) : \frac{d\dot{\epsilon}'}{dt}(t) - B(t), \quad (21)$$

where

$$\hat{A}(t) = 2\mu N \left\{ \hat{\epsilon}(t) - \int_0^t \hat{\epsilon}(\tau) d\tau \int_0^\infty \Gamma(v) \exp[-\Gamma(v)(t - \tau)] p(v) dv \right\}, \quad (22)$$

$$B(t) = \mu \int_0^\infty \Gamma(v) \left\{ n(t, 0, v) \dot{\epsilon}'(t) : \dot{\epsilon}'(t) + \int_0^t \frac{\partial n}{\partial \tau}(t, \tau, v) [\hat{\epsilon}(t) - \hat{\epsilon}(\tau)]' : [\hat{\epsilon}(t) - \hat{\epsilon}(\tau)]' d\tau \right\} dv \geq 0. \quad (23)$$

For isothermal deformation of an incompressible medium, the Clausius–Duhem inequality reads

$$Q = -\frac{dW}{dt} + \frac{\hat{\sigma}'}{\rho} : \frac{d\dot{\epsilon}'}{dt} \geq 0,$$

where Q is internal dissipation per unit mass, and $\hat{\sigma}$ stands for the stress tensor. Substitution of Eq. (21) into this equation implies that

$$Q(t) = \frac{1}{\rho} [\hat{\sigma}'(t) - \rho \hat{A}'(t)] : \frac{d\dot{\epsilon}'}{dt}(t) + B(t) \geq 0. \quad (24)$$

As the function $B(t)$ is non-negative, see Eq. (23), dissipation inequality (24) is satisfied, provided that the expression in the square brackets vanishes. This assertion together with Eq. (22) results in the constitutive equation

$$\hat{\sigma}(t) = -P(t)\hat{I} + 2G \left\{ \dot{\epsilon}'(t) - \int_0^t \dot{\epsilon}'(\tau) d\tau \int_0^\infty \Gamma(v) \exp[-\Gamma(v)(t - \tau)] p(v) dv \right\}, \quad (25)$$

where $P(t)$ is pressure, \hat{I} is the unit tensor, and the shear modulus G is determined by Eq. (2).

Formula (25) describes the time-dependent response of an equivalent network at arbitrary three-dimensional deformations with small strains. This equation implies that in a shear test

with $\hat{\epsilon}(t) = \epsilon(t)\mathbf{e}_1\mathbf{e}_2$, where $\epsilon(t)$ is the shear strain, and \mathbf{e}_m ($m = 1, 2, 3$) are unit vectors of a Cartesian frame, the shear stress $\sigma(t)$ reads

$$\sigma(t) = 2G \left\{ \epsilon(t) - \int_0^t \epsilon(\tau) d\tau \int_0^\infty \Gamma(v) \exp[-\Gamma(v)(t - \tau)] p(v) dv \right\}. \quad (26)$$

It follows from Eq. (26) that in a shear oscillation test with $\epsilon(t) = \epsilon_0 \exp(i\omega t)$, where ϵ_0 and ω are the amplitude and frequency of oscillations, and $i = \sqrt{-1}$, the transient complex modulus $\bar{G}^*(t, \omega) = \sigma(t)/(2\epsilon(t))$ is determined by the formula

$$\bar{G}^*(t, \omega) = G \left\{ 1 - \int_0^\infty \Gamma(v) p(v) dv \int_0^t \exp[-(\Gamma(v) + i\omega)s] ds \right\},$$

where $s = t - \tau$. This equality implies that the steady-state complex modulus $G^*(\omega) = \lim_{t \rightarrow \infty} \bar{G}^*(t, \omega)$ is given by

$$G^*(\omega) = G \int_0^\infty \frac{i\omega}{\Gamma(v) + i\omega} p(v) dv.$$

This equality together with Eq. (12) implies that the steady-state storage $G'(\omega)$ and loss $G''(\omega)$ shear moduli read

$$\begin{aligned} G'(\omega) &= G \int_0^\infty \frac{\omega^2}{\Gamma_0^2 \exp(-2v) + \omega^2} p(v) dv, \\ G''(\omega) &= G \int_0^\infty \frac{\Gamma_0 \exp(-v) \omega}{\Gamma_0^2 \exp(-2v) + \omega^2} p(v) dv. \end{aligned} \quad (27)$$

To fit the experimental data, we adopt the random energy model (Derrida, 1980) with the quasi-Gaussian distribution function $p(v)$,

$$p(v) = p_0 \exp\left[-\frac{(v - V)^2}{2\Sigma^2}\right] \quad (v \geq 0), \quad p(v) = 0 \quad (v < 0), \quad (28)$$

where V and Σ are adjustable parameters (an apparent average activation energy and an apparent standard deviation of activation energies, respectively), and the constant p_0 is found from the normalization condition

$$\int_0^\infty p(v) dv = 1. \quad (29)$$

The average activation energy for separation of strands V_* and the standard deviation of activation energies Σ_* are determined by the conventional formulas

$$V_* = \int_0^\infty v p(v) dv, \quad \Sigma_* = \left[\int_0^\infty (v - V_*)^2 p(v) dv \right]^{\frac{1}{2}}. \quad (30)$$

Governing equations (27) and (28) involve three material constants: (i) the instantaneous shear modulus G , (ii) the average activation energy for rearrangement of strands in a network V_* , and (iii) the standard deviation of activation energies Σ_* . For shear oscillatory tests performed at various temperatures T , these quantities become functions of T . Our purpose now is to find these parameters by matching the observations for $G'(\omega)$ and $G''(\omega)$ depicted in Figures 1 to 4.

4 Fitting of observations

Each set of the experimental data is fitted separately. We fix some intervals $[0, V_{\max}]$ and $[0, \Sigma_{\max}]$, where the “best-fit” parameters V and Σ are assumed to be located, and divide these intervals into J subintervals by the points $V^{(i)} = i\Delta V$ and $\Sigma^{(j)} = j\Delta\Sigma$ ($i, j = 1, \dots, J-1$) with $\Delta V = V_{\max}/J$ and $\Delta\Sigma = \Sigma_{\max}/J$. For any pair $\{V^{(i)}, \Sigma^{(j)}\}$, the coefficient p_0 in Eq. (28) is determined from Eq. (29), where the integral is evaluated numerically by Simpson’s method with 400 points and the step $\Delta v = 0.1$. The integrals in Eq. (27) are calculated by using the same technique. The shear modulus G is found by the least-squares method from the condition of minimum of the function

$$F = \sum_{\omega_m} \left\{ \left[G'_{\text{exp}}(\omega_m) - G'_{\text{num}}(\omega_m) \right]^2 + \left[G''_{\text{exp}}(\omega_m) - G''_{\text{num}}(\omega_m) \right]^2 \right\},$$

where the sum is calculated over all frequencies ω_m at which the data were collected, G'_{exp} and G''_{exp} are the storage and loss moduli measured in a test, and G'_{num} and G''_{num} are given by Eq. (27). The “best-fit” parameters V and Σ are determined from the condition of minimum of the function F on the set $\{V^{(i)}, \Sigma^{(j)}\}$. After finding the “best-fit” values $V^{(i)}$ and $\Sigma^{(j)}$, this procedure is repeated twice for the new intervals $[V^{(i-1)}, V^{(i+1)}]$ and $[\Sigma^{(j-1)}, \Sigma^{(j+1)}]$, to ensure an acceptable accuracy of fitting. Figures 1 to 4 demonstrate good agreement between the experimental data and the results of numerical simulation.

After finding the instantaneous shear modulus G of iPP and LDPE, we calculate the parameter l_e by using Eq. (5) and plot this quantity versus temperature T in Figure 5. To demonstrate the level of discrepancies between the values of l_e measured on different specimens, experimental data are presented for two sets of observations on iPP. The dependence $l_e(T)$ is approximated by Eq. (8), where the coefficients $l_e^{(m)}$ ($m = 0, 1$) are determined by the least-squares technique. Figure 5 shows that Eq. (8) provides fair approximation of the observations. The average contour length between entanglements l_e grows with temperature T . The rate of increase in $l_e(T)$ is more pronounced for iPP than for LDPE.

Given adjustable parameters V and Σ determined at each test temperature T , we calculate the dimensionless average activation energy for separation of strands from temporary junctions V_* and the dimensionless standard deviation of activation energies Σ_* by formulas (30), where the integrals are evaluated numerically. The average activation energy \bar{V}_* and the standard deviation of activation energies $\bar{\Sigma}_*$ are found from the equations similar to Eq. (11),

$$\bar{V}_* = k_B T V_*, \quad \bar{\Sigma}_* = k_B T \Sigma_*.$$

The average activation energy \bar{V}_* is depicted versus temperature T in Figure 6. The experimental data are approximated by the linear equation

$$\bar{V}_* = (V_0 + V_1 T) \cdot 10^{-19}, \quad (31)$$

where the coefficients V_m ($m = 0, 1$) are determined by the least-squares method. Figure 6 demonstrates that Eq. (31) correctly describes the evolution of \bar{V}_* with temperature. The average activation energy for rearrangement of strands \bar{V}_* grows with temperature for both polymers. The rate of increase is more pronounced for LDPE than for iPP. Given a temperature T , the average activation energy for separation of strands in iPP noticeably exceeds that in LDPE.

The standard deviation of activation energies $\bar{\Sigma}_*$ is plotted versus temperature T in Figure 7. The experimental data are approximated by the linear function

$$\bar{\Sigma}_* = (\Sigma_0 + \Sigma_1 T) \cdot 10^{-19}, \quad (32)$$

where the coefficients Σ_m ($m = 0, 1$) are determined by the least-squares technique. Figure 7 reveals that Eq. (32) adequately describes changes in $\bar{\Sigma}_*$ with temperature. The standard deviation of activation energies $\bar{\Sigma}_*$ slightly increases with T for iPP and weakly decreases with temperature for LDPE. Given a temperature T , the standard deviation of activation energies for LDPE substantially exceeds that for iPP.

To assess the effect of temperature T on the average relaxation time τ_0 , we calculate the modulus of complex viscosity η by the standard formula

$$\eta(\omega) = \left[(G'(\omega))^2 + \left(\frac{G''(\omega)}{\omega} \right)^2 \right]^{\frac{1}{2}}, \quad (33)$$

and find the zero-frequency complex viscosity $\eta_0 = \lim_{\omega \rightarrow 0} \eta(\omega)$. It follows from Eqs. (27) and (33) that

$$\eta_0 = \frac{G}{\Gamma_0} \int_0^\infty \exp(v) p(v) dv. \quad (34)$$

The average relaxation time τ_0 is given by

$$\tau_0 = \frac{\eta_0}{G}.$$

Substitution of expression (35) into this equality results in

$$\tau_0 = \frac{1}{\Gamma_0} \int_0^\infty \exp(v) p(v) dv. \quad (35)$$

For any temperature under consideration T , we calculate the integral in Eq. (35) by Simpson's method with 400 points and the step $\Delta v = 0.1$. The distribution function $p(v)$ is given by Eq. (28) with the parameters V and Σ found by fitting the experimental data for $G'(\omega)$ and $G''(\omega)$. The average relaxation time τ_0 is plotted versus temperature T in Figure 8. The experimental data are approximated by the Arrhenius dependence

$$\tau_0 = \tau_* \exp\left(\frac{E}{RT}\right), \quad (36)$$

where τ_* is the average relaxation time at elevated temperatures ($T \rightarrow \infty$), E is the activation energy, and R is the universal gas constant. To match the observations, we present Eq. (36) in the form

$$\ln \tau_0 = \tau_0^{(0)} + \frac{\tau_0^{(1)}}{T} \quad (37)$$

with

$$\tau_0^{(0)} = \ln \tau_*, \quad \tau_0^{(1)} = \frac{E}{R}. \quad (38)$$

Figure 8 demonstrates that Eq. (37), where the coefficients $\tau_0^{(m)}$ ($m = 0, 1$) are determined by the least-squares technique, adequately describes the experimental data for both polymers.

5 Discussion

Figure 5 shows the average contour length between entanglements l_e strongly increases with temperature for both polyolefins under investigation. The characteristic temperature for disentanglement T_e of LDPE exceeds that of iPP by about twice. To calculate the coefficient α_e in Eq. (7), we use Eq. (8) and the results of numerical analysis and find $\alpha_e = 0.023 \text{ K}^{-1}$ for iPP and $\alpha_e = 0.013 \text{ K}^{-1}$ for LDPE. This means that l_e changes rather weakly with temperature for a highly branched polymer melt, and it is strongly affected by temperature for a melt with relatively short branches.

This finding may be explained based on the following scenario. Slightly above its melting temperature T_m , polypropylene chains are closely packed, which implies that the number of macromolecules that intersect a volume occupied by an individual chain is relatively large (a high average number of entanglements per chain and a small distance between entanglements l_e). With the growth of temperature, thermal oscillations of segments induce loosening of this packaging and an increase in the occupied volume. Some macromolecules that crossed the occupied volume for an individual chain near the melting point are forced to leave this volume with an increase in T . This results in a substantial decrease in the number of entanglements per chain and a strong exponential growth of l_e .

On the contrary, due to the presence of long branches, packaging of chains in LDPE at the temperatures T close to its melting temperature T_m is relatively loose. This poor packaging is associated with formation of physical cross-links (knots) between long branches and between long branches and the backbones of polyethylene chains (in addition to entanglements between backbones). The growth of temperature induces partial disentanglement of junctions formed by long branches, which implies that the main chains become more closely packed (the latter is reflected by the fact that the coefficient of thermal expansion of LDPE is negative). Although the total number of entanglements between chains is reduced with temperature, the rate of increase in $l_e(T)$ in LDPE is weaker than that in iPP, in agreement with the experimental data depicted in Figure 5.

Figure 6 demonstrates that the average activation energy for separation of strands from temporary junctions \bar{V}_* slightly grows with temperature for iPP. This increase may be associated with the fact that disentanglement of chains driven by the growth of temperature begins with relatively weak junctions (that are characterized by small activation energies). The latter means that the average activation energy of an ensemble of chains increases due to disappearance of “weak” junctions untangled under heating.

The rate of growth of the average activation energy \bar{V}_* of LDPE with temperature T is substantially stronger than that of iPP. This may be explained by the fact that an increase in temperature induces breakage of physical cross-links between long branches and between long branches and backbones in LDPE (which are characterized by relatively low activation energies). As a result of thermally-induced destruction of “weak” junctions, only relatively strong knots between backbones survive. Because these “strong” entanglements have high activation energies, the average activation energy of an ensemble pronouncedly increases with temperature.

According to Figure 6, the average activation energy \bar{V}_* of iPP substantially exceeds that of LDPE. This conclusion appears to be natural, because the activation energy of a junction is determined by local properties of entangled chains. The strength of a knot formed by two

chains is relatively low for LDPE (interactions between backbones of linear chains), and it is noticeably higher for iPP due to additional interactions between methyl side-groups belonging to different chains.

Figure 7 shows that the standard deviations of activation energies $\bar{\Sigma}_*$ of iPP and LDPE are weakly affected by temperature. The parameter $\bar{\Sigma}_*$ slightly increases with temperature for iPP (due to partial disentanglement of backbones), and it slightly decreases with T for LDPE (driven by breakage of weak junctions between long branches). Given a temperature T , the standard deviation of activation energies of LDPE substantially exceeds $\bar{\Sigma}_*$ of iPP. This finding seems quite natural, because the presence of “weak” physical cross-links between long branches implies a broad distribution of activation energies for rearrangement of strands.

Figure 8 reveals that the average relaxation time τ_0 grows with temperature for both polymers under consideration. Given $\tau_0^{(1)}$, we calculate the activation energy E from Eq. (38) and find $E = 10.4$ kcal/mol for iPP and $E = 18.1$ kcal/mol for LDPE. These values are in good accord with the activation energies provided by other researchers for polypropylene: $E = 9.3$ kcal/mol (Eckstein et al., 1998), $E = 9.7 - 10.0$ kcal/mol (Pearson et al., 1988), $E = 10.0$ kcal/mol (Fujiyama et al., 2002), and low-density polyethylene: $E = 9.1 - 13.2$ kcal/mol (Wood-Adams and Costeaux, 2001), $E = 13.5$ kcal/mol (Qiu and Ediger, 2000).

6 Concluding remarks

Two series of torsional oscillation tests have been performed on melts of isotactic polypropylene and low-density polyethylene in the range of temperatures between 170 and 250 °C (iPP) and between 120 and 190 °C (LDPE).

With reference to the concept of transient networks, constitutive equations have been developed for the viscoelastic response of polymer melts at isothermal three-dimensional deformations with small strains. The melt is treated as an equivalent transient network of strands bridged by temporary junctions. Its time-dependent behavior is modelled as thermally-activated separation of active strands from their junctions and attachment of dangling strands to the network. Stress-strain relations for an equivalent heterogeneous network of strands (where different junctions have different activation energies for rearrangement of strands) have been derived by using the laws of thermodynamics. These equations involve three material parameters that are determined by matching the experimental data for the storage and loss moduli as functions of frequency of oscillations. Fair agreement is demonstrated between the observations and the results of numerical simulation.

The following conclusions are drawn:

1. The average contour length between entanglements l_e grows with temperature T for both polyolefins under consideration. Thermally-induced changes in $l_e(T)$ are correctly described by Eq. (7). The relative rate of increase in $l_e(T)$ is higher for iPP than for LDPE.
2. The average activation energy for rearrangement of strands \bar{V}_* grows with temperature due to breakage of “weak” junctions between chains. The rate of increase in \bar{V}_* for LDPE exceeds than for iPP (due to thermally-induced destruction of knots between long

branches). Given a temperature T , the average activation energy of iPP is substantially higher than that of LDPE (due to local interactions between methyl side-groups).

3. The standard deviation of activation energies for separation of active strands $\bar{\Sigma}_*$ is weakly affected by temperature. The value of $\bar{\Sigma}_*$ for LDPE noticeably exceeds that for iPP (which reflects the fact that the presence of “weak” physical cross-links between long branches in polyethylene results in a very broad distribution of activation energies).

An explicit expression (35) is derived for the average relaxation time τ_0 . It is demonstrated that the activation energies of iPP and LDPE calculated by using Eqs. (35) and (36) are close to those reported in the literature.

Acknowledgement

This work was partially supported by the West Virginia Research Challenge Grant Program.

References

- de Gennes PG (1979) Scaling concepts in polymer physics. Cornell Univ. Press, Ithaca
- Derrida B (1980) Random-energy model: limit of a family of disordered models. *Phys Rev Lett* 45: 79–92
- Drozdov AD, Christiansen JdeC. (2003) The effect of annealing on the viscoplastic response of semicrystalline polymers at finite strains. *Int J Solids Struct* 40: 1337–1367.
- Eckstein A, Suhm J, Friedrich C, Maier R-D, Sassmannshausen J, Bochmann M, Mülhaupt R (1998) Determination of plateau moduli and entanglement molecular weights of isotactic, syndiotactic, and atactic polypropylenes synthesized with metallocene catalysis. *Macromolecules* 31: 1335–1340
- Eyring H (1936) Viscosity, plasticity, and diffusion as examples of absolute reaction rates. *J Chem Phys* 4: 283–291
- Ferry JD (1980) Viscoelastic properties of polymers. Wiley, New York
- Fujiyama M, Kitajima Y, Inata H (2002) Rheological properties of polypropylenes with different molecular weight distribution characteristics. *J Appl Polym Sci* 84: 2128–2141
- Green MS, Tobolsky AV (1946) A new approach to the theory of relaxing polymeric media. *J Chem Phys* 14: 80–92
- Lodge AS (1968) Constitutive equations from molecular network theories for polymer solutions. *Rheol Acta* 7: 379–392
- Pearson DS, Fetters LJ, Younghouse LB, Mays JW (1988) Rheological properties of poly(1,3-dimethyl-1-butenylene) and model atactic polypropylene. *Macromolecules* 21: 478–484
- Qiu X, Ediger MD (2000) Branching effects on the segmental dynamics of polyethylene melts. *J Polym Sci Part B: Polym Phys* 38: 2634–2643
- Richter D, Farago B, Fetters LJ, Huang JS, Ewen B, Lartigue C (1990) Direct microscopic observation of the entanglement distance in a polymer melt. *Phys Rev Lett* 64: 1389–1392
- Richter D, Farago B, Butera R, Fetters LJ, Huang JS, Ewen B (1993) On the origins of entanglement constraints. *Macromolecules* 26: 795–804
- Sweeney J, Collins TLD, Coates PD, Duckett RA (1999) High temperature large strain viscoelastic behaviour of polypropylene modeled using an inhomogeneously strained network. *J Appl Polym Sci* 72: 563–575
- Tanaka F, Edwards SF (1992) Viscoelastic properties of physically cross-linked networks. Transient network theory. *Macromolecules* 25: 1516–1523
- Wood-Adams P, Costeux S (2001) Thermorheological behavior of polyethylene: effects of microstructure and long chain branching. *Macromolecules* 34: 6281–6290
- Yamamoto M (1956) The visco-elastic properties of network structure. 1. General formalism. *J Phys Soc Japan* 11: 413–421

List of figures

Figure 1: The storage modulus G' versus frequency ω . Circles: experimental data on iPP at the temperatures $T = 190, 210, 230$ and 250 °C, from top to bottom, respectively. Solid lines: results on numerical simulation

Figure 2: The loss modulus G'' versus frequency ω . Circles: experimental data on iPP at the temperatures $T = 190, 210, 230$ and 250 °C, from top to bottom, respectively. Solid lines: results on numerical simulation

Figure 3: The storage modulus G' versus frequency ω . Circles: experimental data on LDPE at the temperatures $T = 120, 130, 140, 150, 160, 170, 180$ and 190 °C, from top to bottom, respectively. Solid lines: results on numerical simulation

Figure 4: The loss modulus G'' versus frequency ω . Circles: experimental data on LDPE at the temperatures $T = 120, 130, 140, 150, 160, 170, 180$ and 190 °C, from top to bottom, respectively. Solid lines: results on numerical simulation

Figure 5: The parameter l_e versus temperature T . Symbols: treatment of observations on iPP (unfilled circles) and LDPE (filled circles). Solid lines: approximation of the experimental data by Eq. (8). Curve 1: $l_e^{(0)} = 1.09$, $l_e^{(1)} = 1.04 \cdot 10^{-5}$, $T_0 = 43.2$. Curve 2: $l_e^{(0)} = -0.09$, $l_e^{(1)} = 1.30 \cdot 10^{-3}$, $T_0 = 77.2$

Figure 6: The average activation energy \bar{V}_* versus temperature T . Symbols: treatment of observations on iPP (unfilled circles) and LDPE (filled circles). Solid lines: approximation of the experimental data by Eq. (31). Curve 1: $V_0 = 4.42 \cdot 10^3$, $V_1 = 16.41$. Curve 2: $V_0 = -1.06 \cdot 10^4$, $V_1 = 40.22$

Figure 7: The standard deviation of activation energies $\bar{\Sigma}_*$ versus temperature T . Symbols: treatment of observations on iPP (unfilled circles) and LDPE (filled circles). Solid lines: approximation of the experimental data by Eq. (32). Curve 1: $\Sigma_0 = 1.01 \cdot 10^3$, $\Sigma_1 = 1.79$. Curve 2: $\Sigma_0 = 3.36 \cdot 10^3$, $\Sigma_1 = -9.52$

Figure 8: The average relaxation time τ_0 versus temperature T . Symbols: treatment of observations on iPP (unfilled circles) and LDPE (filled circles). Solid lines: approximation of the experimental data by Eq. (37). Curve 1: $\tau_0 = -13.74$, $\tau_1 = 5.24 \cdot 10^3$. Curve 2: $\tau_0 = -22.18$, $\tau_1 = 9.12 \cdot 10^3$

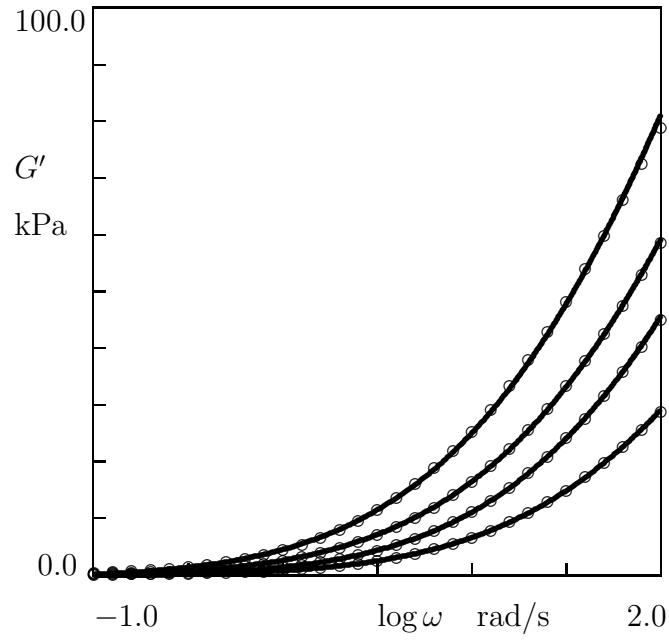


Figure 1:

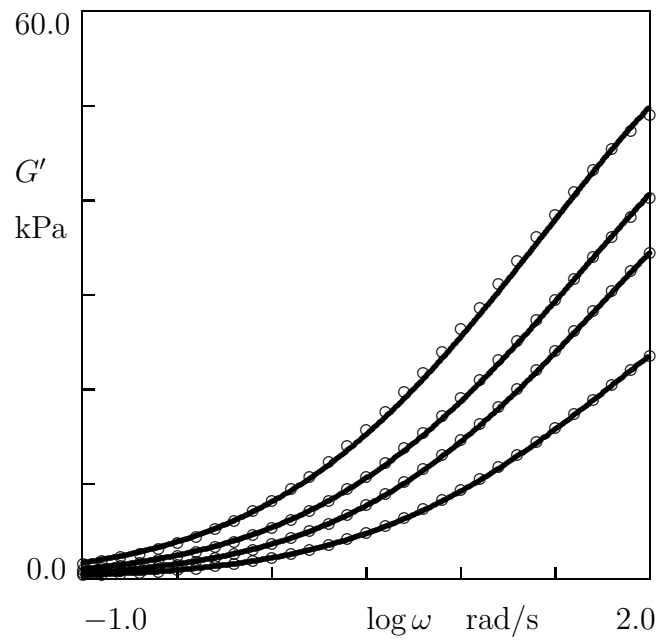


Figure 2:

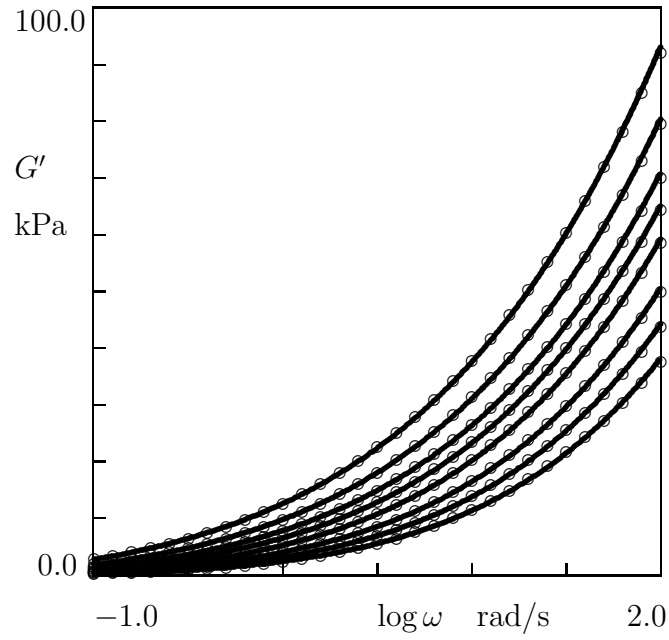


Figure 3:

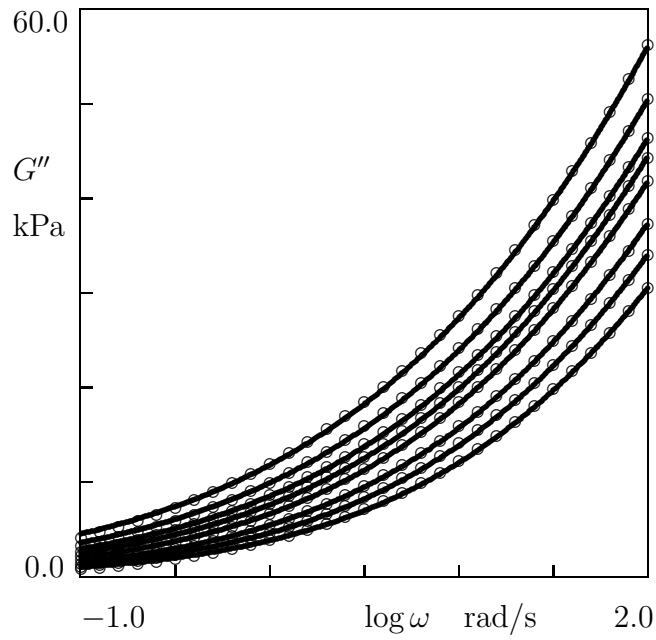


Figure 4:

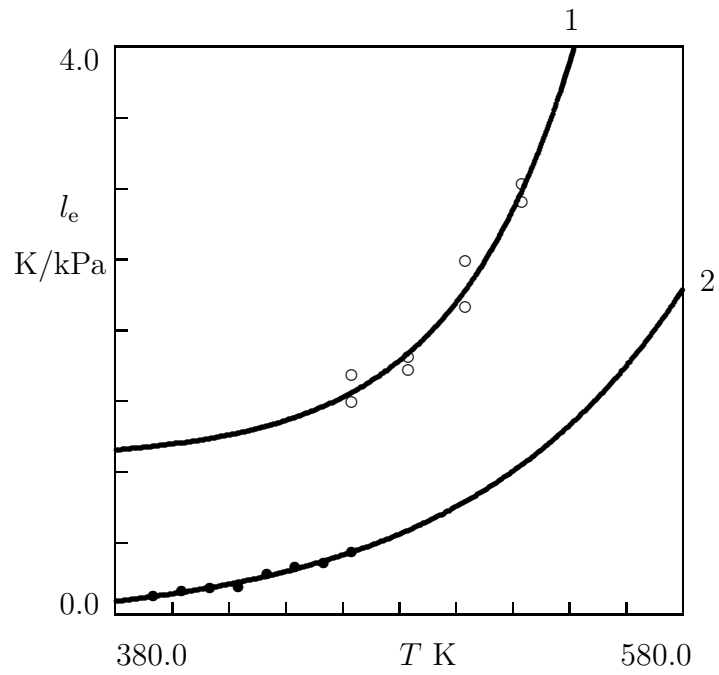


Figure 5:

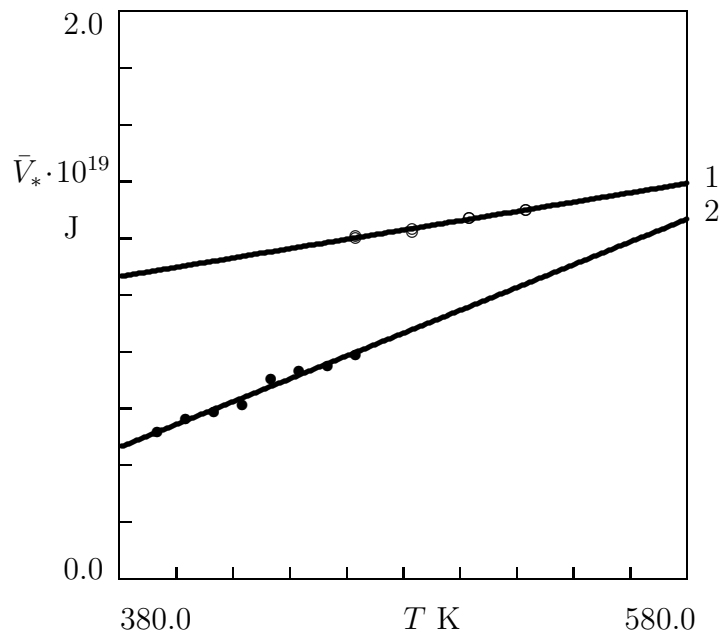


Figure 6:

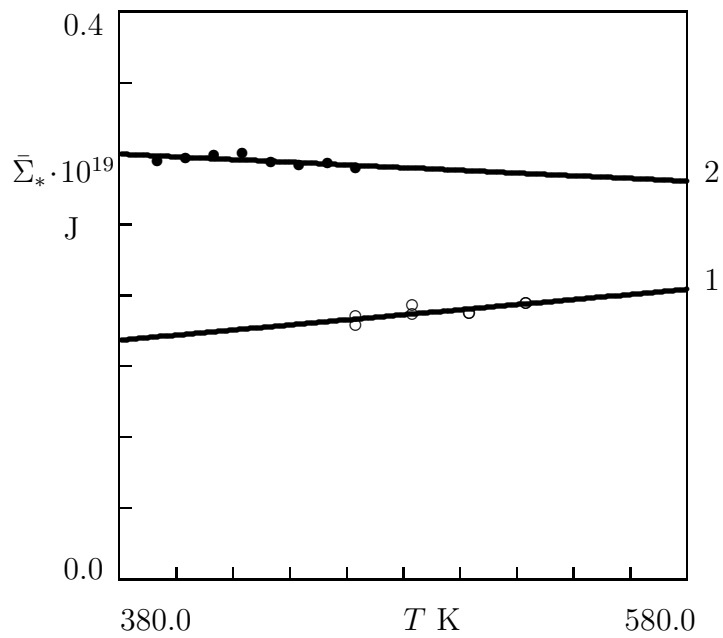


Figure 7:

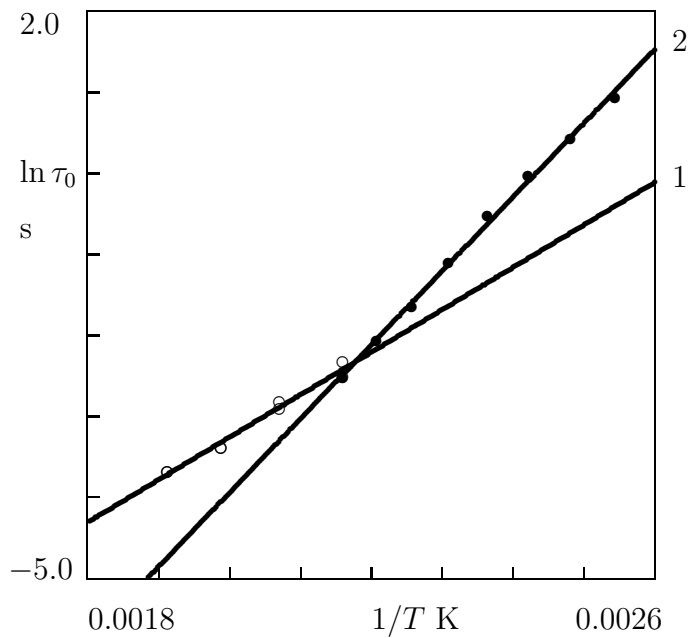


Figure 8: